

# A linear magnetic flux-to-voltage transfer function of differential DC SQUID

I I Soloviev<sup>1,2,3,4</sup>, V I Ruzhickiy<sup>1,3,4,5</sup>, N V Klenov<sup>1,2,3,4,5</sup>, S V Bakurskiy<sup>1,2,3,4</sup> and M Yu Kupriyanov<sup>1,2</sup>

<sup>1</sup>Lomonosov Moscow State University Skobeltsyn Institute of Nuclear Physics, 119991, Moscow, Russia

<sup>2</sup>Moscow Institute of Physics and Technology, State University, 141700 Dolgoprudny, Moscow region, Russia

<sup>3</sup>MIREA - Russian Technological University, 119454, Moscow, Russia

<sup>4</sup>N. L. Dukhov All-Russia Research Institute of Automatics, 127055, Moscow, Russia

<sup>5</sup>Physics Department, Moscow State University, 119991, Moscow, Russia

E-mail: isol@phys.msu.ru

**Abstract.** A superconducting quantum interference device with differential output or “DSQUID” was proposed earlier for operation in the presence of large common-mode signals. The DSQUID is the differential connection of two identical SQUIDs. Here we show that besides suppression of electromagnetic interference this device provides effective linearization of DC SQUID voltage response. In the frame of the resistive shunted junction model with zero capacitance, we demonstrate that Spur-Free Dynamic Range (SFDR) of DSQUID magnetic flux-to-voltage transfer function is higher than SFDR > 100 dB while Total Harmonic Distortion (THD) of a signal is less than THD < 10<sup>-3</sup>% with a peak-to-peak amplitude of a signal being a quarter of half flux quantum,  $2\Phi_a = \Phi_0/8$ . Analysis of DSQUID voltage response stability to a variation of the circuit parameters shows that DSQUID implementation allows doing highly linear magnetic flux-to-voltage transformation at the cost of a high identity of Josephson junctions and high-precision current supply.

PACS numbers: 85.25.Dg, 85.25.Am

*Keywords:* DC SQUID, voltage response, linearity, working margins, DSQUID

## 1. Introduction

Modern Josephson junction fabrication technology [1, 2] allows the development of complex circuits [3] with high-precision control of their parameters. Both low-temperature and high-temperature superconductor (LTS and HTS) technology provide a possibility to fabricate SQUID arrays with the number of Josephson junctions about a million [4, 5]. This expands the area of SQUID applications to the one where SQUID-based structures should ideally act as a linear magnetic flux-to-voltage transformers [5–11]: from electrically small antennas to analog-to-digital convertor circuits and from susceptometers to SQUID-based multiplexers.

SQUID-based structures with high dynamic range and highly linear voltage response obtained without a feedback loop were named the “superconducting quantum arrays” (SQA) [12–14]. Two types of cells were proposed as basic blocks of SQA. These are the bi-SQUID [15–22] and the so-called differential quantum cell (DQC) [6, 12–14, 23–27]. Unfortunately, despite several attempts to realization of bi-SQUID-based structures [17, 28, 29] no outstanding results were reported [22]. DQC seems to deliver better performance for SQA [6]. However, since DQC is a differential connection of identical parallel SQUID arrays, it usually occupies a large area which is not convenient in some cases.

In this paper, we consider the simplest version of DQC - two identical DC SQUIDs with a differential output which we call a “DSQUID”, see Fig. 1a. Earlier it was shown that the DSQUID allows obtaining high common-mode rejection ratio [30]. This feature is especially useful where SQUID-based system contains long wiring. It was also noted that the effects of background magnetic fields and of temperature fluctuations are also suppressed due to this differential configuration. [30].

Here we show that besides the presented advantages the DSQUID possesses high voltage response linearity of DQC. We report the range of DSQUID parameters providing high linearity of its voltage response as well as analysis of the linearity decrease with deviation of the circuit parameters from their optimal values.

## 2. Model

DSQUID voltage response is obtained by subtraction of voltage responses of its parts:  $u_\Sigma = u_+ - u_-$ , see

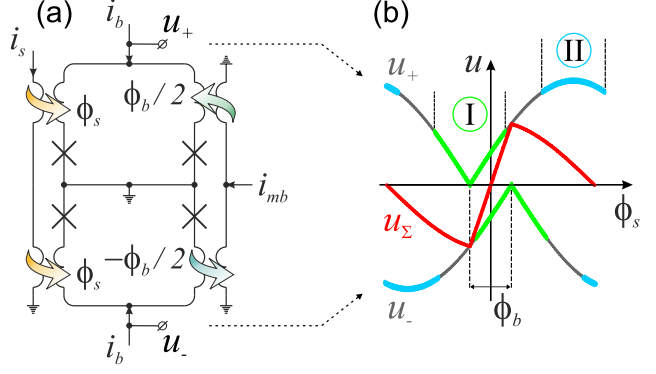


**Figure 1.** (a) DSQUID scheme.  $i_b$  is the bias current,  $i_s$  is the signal current providing the signal flux,  $\phi_s$ , and  $i_{mb}$  is the magnetic bias current providing the bias flux,  $\phi_b$ . DSQUID voltage response  $u_\Sigma$  is obtained between nodes  $u_\pm$ . (b) Sketch of DSQUID voltage response formation as subtraction of voltage responses of its parts:  $u_\Sigma = u_+ - u_-$ . DC SQUID voltage response regions linearized in DSQUID are marked by numbers I and II.

Fig. 1. Josephson junctions of DSQUID ought to be overdamped to accomplish the high linearity of DQC [6]. Equality of DSQUID parts naturally suggests the using of LTS technology where the technological spread of parameters can be minimized. For the temperature  $T = 4.2$  K the effective current noise value is  $I_T = (2\pi/\Phi_0)k_B T \approx 0.18 \mu\text{A}$ , where  $\Phi_0$  is the magnetic flux quantum and  $k_B$  is the Boltzmann constant. The choice of Josephson junction critical current  $I_c \geq 180 \mu\text{A}$  leads to dimensionless noise intensity  $\gamma = I_T/I_c \leq 10^{-3}$  which makes the noise impact to DQC characteristics to be insignificant [6]. Transfer function of each SQUID of DSQUID is calculated in the frame of the well-known Resistive Shunted Junction (RSJ) model with zero capacitance, accordingly. The system of equations describing SQUID in terms of Josephson phase sum and difference  $\varphi_\pm = (\varphi_1 \pm \varphi_2)/2$  (where  $\varphi_{1,2}$  are Josephson phases of SQUID junctions) is as follows:

$$\frac{d\varphi_+}{d\tau} = i_b - \sin \varphi_+ \cos \varphi_-, \quad (1a)$$

$$\frac{d\varphi_-}{d\tau} = -(\varphi_- - \varphi_e)/\beta_l - \sin \varphi_- \cos \varphi_+, \quad (1b)$$

where time  $\tau = t\omega_c$  is normalized to the characteristic frequency  $\omega_c = 2\pi I_c R_n/\Phi_0$ ,  $R_n$  is the junction shunt resistance,  $i_b = I_b/2I_c$  is the normalized bias current,  $\beta_l = \pi L I_c/\Phi_0$  is the normalized SQUID inductance,

and  $\phi_e = \pi\Phi_e/\Phi_0$  is the normalized applied magnetic flux. For each SQUID of DSQUID  $\phi_e$  is the sum of the signal flux,  $\phi_s$ , and the magnetic bias flux setting the working point and the width of the working region,  $\pm\phi_b/2$ , as it is shown in Fig. 1.

We use two approaches for estimation of voltage response linearity. The first one is calculation of so-called Spur-Free Dynamic Range (SFDR). In this approach we apply the external magnetic flux to each SQUID of DSQUID in the form,

$$\phi_e = (\phi_a/2) \sin \omega_1 \tau + (\phi_a/2) \sin \omega_2 \tau \pm \phi_b/2, \quad (2)$$

where frequencies  $\omega_2 = 1.1\omega_1$  are much smaller than Josephson oscillation frequency,  $\omega_{1,2} \ll \omega_J$ ,  $\phi_a$  is the amplitude of signal. SFDR is calculated as a ratio of one of the signal tones to maximum amplitude of distortions arising in spectrum of output signal due to nonlinearity of magnetic flux-to-voltage transfer function.

The second approach is calculation of Total Harmonic Distortion (THD). In this case the applied signal contains only one harmonic component:

$$\phi_e = \phi_a \sin \omega \tau \pm \phi_b/2. \quad (3)$$

THD is calculated as  $\text{THD} = \sqrt{\sum_{n=2}^{\infty} A_n^2}/A_1$ , where  $A_n$  are amplitudes of output signal spectral harmonics.

SFDR and THD calculation requires finding the accurate shape of DSQUID voltage response by numerical solutions of system (1) for each SQUID. For this purpose we define the dependence  $\varphi_-(\varphi_+)$  combining equations (1a,b),

$$\frac{d\varphi_-}{d\varphi_+} = \frac{-(\varphi_- - \phi_e)/\beta_l - \sin \varphi_- \cos \varphi_+}{i_b - \sin \varphi_+ \cos \varphi_-}, \quad (4)$$

and then calculate the period of Josephson oscillations using (1a):

$$T = \int_0^{2\pi} \frac{d\varphi_+}{i_b - \sin \varphi_+ \cos \varphi_-(\varphi_+)}. \quad (5)$$

This gives us the Josephson oscillation frequency,  $\omega_J = 2\pi/T$ , which is equal to time-averaged voltage,  $u$ , normalized to  $I_c R_n$  product.

Calculation of voltage response shape for estimation of magnetic flux-to-voltage transfer coefficient is done much faster using analytical expressions presented in [31, 32].

### 3. Linearization

Differential connection of two identical SQUIDs in DSQUID with their mutual flux bias allows subtraction of some part of SQUID voltage response from its mirrored image, see Fig. 1b, due to symmetry and periodicity of SQUID voltage response. This subtraction leads to partial compensation of nonlinear terms in DSQUID magnetic flux-to-voltage transfer

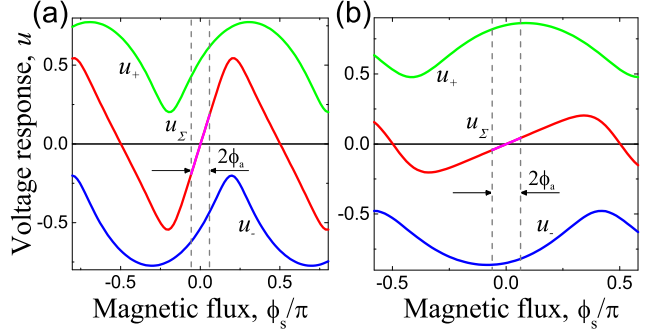


**Figure 2.** DSQUID voltage response,  $u_\Sigma$ , and voltage responses of its parts,  $u_\pm$ , for the following sets of parameters: (a)  $i_b = 1.02$ ,  $\beta_l = 0.35\pi$ ,  $\phi_b = 0.3895\pi$  and (b)  $i_b = 1.108$ ,  $\beta_l = 0.35\pi$ ,  $\phi_b = 0.8337\pi$ . Boundaries of the linear range of the total voltage response  $u_\Sigma$  are marked by vertical dotted lines. Linearity of the linear range is (a) SFDR = 92 dB, THD =  $6 \cdot 10^{-3}\%$  and (b) SFDR = 112 dB, THD =  $6 \cdot 10^{-4}\%$ . The width of the linear range in both cases corresponds to  $2\phi_a \approx \pi/8$ .

function for two regions of SQUID voltage response marked by numbers I and II in Fig. 1b.

The first region (I in Fig. 1b) is in the vicinity of zero external magnetic flux ( $\phi_e \approx 0$ ) [31]. In the limit of zero SQUID inductance,  $\beta_l = 0$ , and for the bias current equals the critical current,  $i_b = 1$ , SQUID voltage response shape is described by the function:  $u = |\sin \phi_e|$ . For the bias flux  $\phi_b \leq \pi/2$  and inside the region  $\phi_s \in [-\phi_b/2, \phi_b/2]$  the voltage responses of DSQUID arms can be written as  $u_\pm = \pm \sin(\phi_s \pm \phi_b/2)$ . Thus, in the range where sine can be approximated by a linear function the total response becomes linear:

$$u_\Sigma \approx 2\phi_s \cos \phi_b/2. \quad (6)$$

It is seen that the most linear part of the voltage response (at  $\phi_e = 0$ ) is moved from the boundary of SQUID working region ( $0 \leq \phi_e \leq \pi/2$ ) to its center in DSQUID, making its utilization possible. At the same time the bias flux providing maximum transfer coefficient,  $\phi_b = 0$ , simultaneously makes the width of the working (and linearized) region to be vanishing.

The second region (II in Fig. 1b) suitable for linearization in DSQUID is located near the opposite boundary of SQUID working region ( $\phi_e \approx \pi/2$ ). Analytical approximation of SQUID voltage response found in [31, 32] is

$$u = u_0 - a [1 + (\beta_l^* u_0)^{-2}]^{-1} (i_b - u_0) \tan^2 \phi_e, \quad (7)$$

where  $u_0 = \sqrt{i_b^2 - \cos^2 \phi_e}$  is the voltage response in the limit of vanishing inductance,  $\beta_l = 0$ , and  $a, \beta_l^*$  are parameters depended on  $i_b, \beta_l$  (see Appendix).

In the vicinity of  $\phi_e = \pi/2$  expression (7) can be accurately represented by a Taylor series limited to quadratic term:

$$\lim_{\phi_e \rightarrow \pi/2} u \approx i_b - \frac{1}{2i_b} \left( Q + (1 - QZ) \left[ \phi_e - \frac{\pi}{2} \right]^2 \right). \quad (8)$$

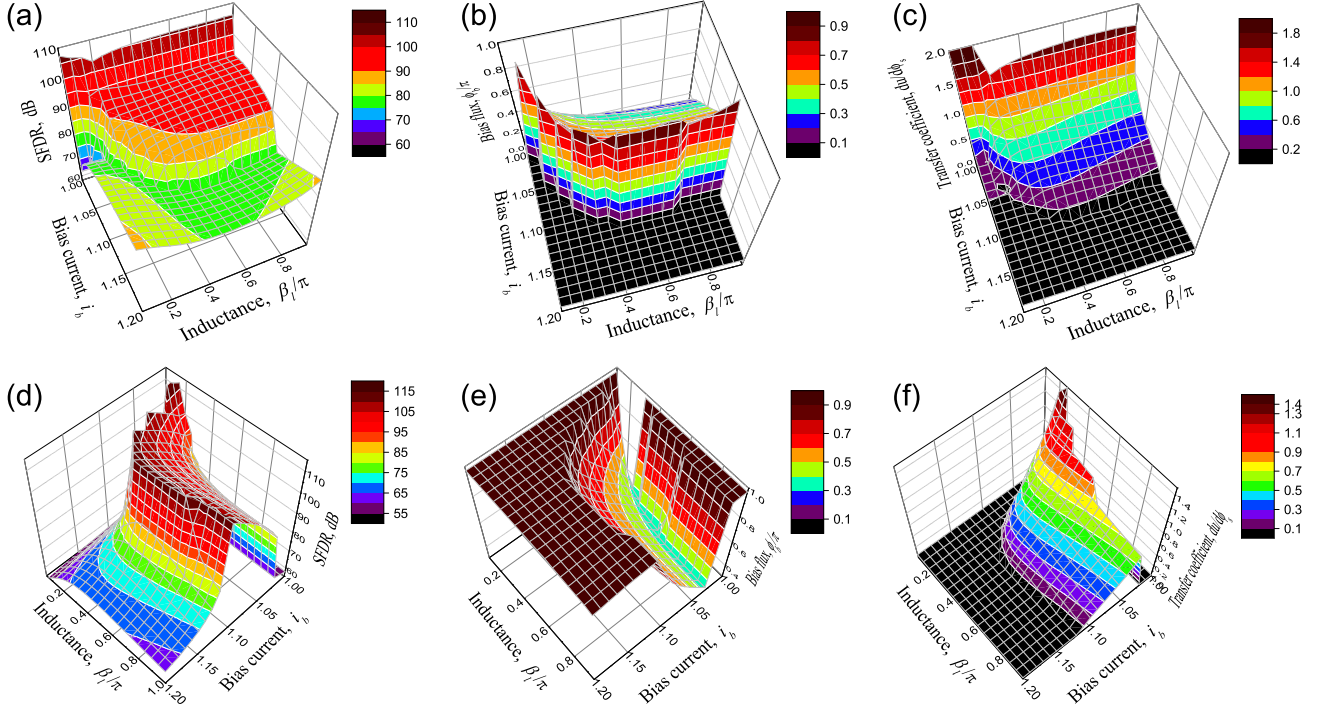


**Figure 3.** Results of the bias flux optimization for obtaining the highest SFDR of DSQUID voltage response under different conditions: (i)  $2\phi_a = 0.3\phi_b$  for (a), (b), (c) and (ii)  $2\phi_a = \pi/8$  for (d), (e), (f). SFDR is presented in (a), (d) planes, the optimal bias flux  $\phi_b/\pi$  is in (b), (e) planes, and the transfer coefficient  $du/d\phi_s$  is in (c), (f).

Dependencies of  $Q$  and  $Z$  on  $i_b, \beta_l$  are presented in the Appendix.

For the bias flux close to  $\phi_b = \pi$  voltage response of DSQUID arms can be written as  $u_{\pm} = u(\phi_s + \pi/2 \mp \delta)$ , where  $\delta = \pi/2 - \phi_b/2$ , due to symmetry of SQUID voltage response. According to (8) this leads to linearized total response:

$$u_{\Sigma} = \phi_s \frac{\pi - \phi_b}{i_b} (1 - QZ). \quad (9)$$

While the width of the region II is defined by the range of validity of approximation (8), the width of the linearized region of DSQUID voltage response is determined by overlapping of the regions II i.e. by the bias flux  $\phi_b$ . Deviation of the bias flux from  $\phi_b = \pi$  increases the transfer coefficient but decreases the linearized region width.

Therefore, in both considered cases we face a tradeoff between the transfer coefficient and the width of linearized region of DSQUID voltage response. Below we show that it is possible to satisfy this tradeoff for the bias flux values in the vicinity of  $\phi_b = 0$  or  $\pi$ . Corresponding examples shown in Fig. 2 are discussed in more detail below.

#### 4. Optimization of parameters

Optimization procedure is performed in the range of the bias current,  $i_b \in [1, 1.2]$ , and the inductance,

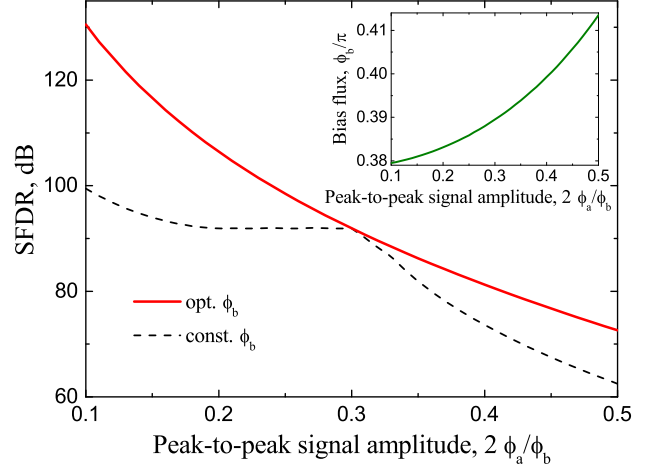


**Figure 4.** SFDR of DSQUID voltage response versus peak-to-peak signal amplitude for chosen values of parameters,  $i_b = 1.02$ ,  $\beta_l = 0.35\pi$ , and optimal bias flux presented in inset (solid line). SFDR for the constant bias flux,  $\phi_b = 0.3895\pi$ , is shown by dotted line.

$\beta_l/\pi \in [0.05, 1]$ . Using standard Nelder-Mead simplex algorithm [33] we numerically find the optimal bias flux providing the highest SFDR of DSQUID voltage response.

We use two different conditions to consider linearization of the two SQUID voltage response

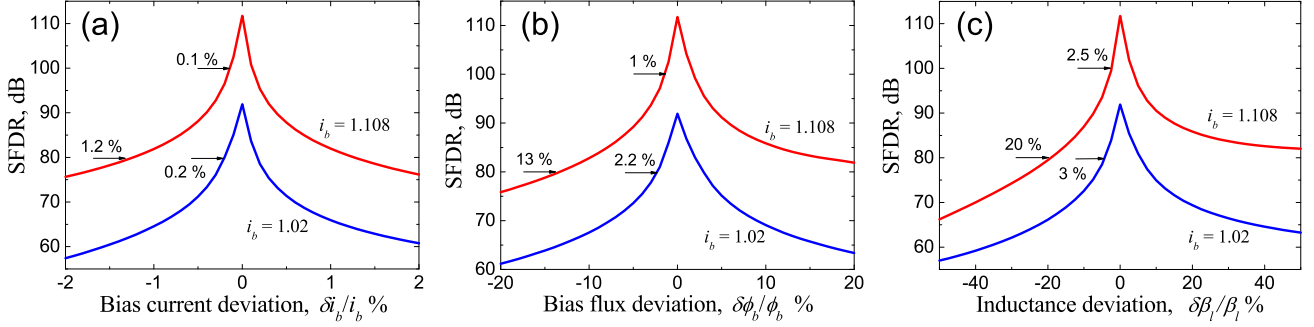


**Figure 5.** SFDR of DSQUID voltage response versus deviation of (a) the bias current,  $\delta i_b/i_b$ , (b) the bias flux,  $\delta \phi_b/\phi_b$ , and (c) the inductance,  $\delta \beta_l/\beta_l$ , for two chosen sets of parameters: (i)  $i_b = 1.02$ ,  $\beta_l = 0.35\pi$ ,  $\phi_b = 0.3895\pi$  and (ii)  $i_b = 1.108$ ,  $\beta_l = 0.35\pi$ ,  $\phi_b = 0.8337\pi$  (corresponding lines are marked by  $i_b$  values).

regions (I and II in Fig. 1b). The first one is limitation of peak-to-peak signal to 30% of the width of DSQUID working region,  $2\phi_a = 0.3\phi_b$ . It is used to consider utilization of the region I ( $\phi_e \approx 0$ ). The usage of the region II ( $\phi_e \approx \pi/2$ ) is considered with limitation of peak-to-peak signal to a fixed value equal to a quarter of SQUID working region,  $2\phi_a = \pi/8$ .

Results of optimization obtained with utilization of the first condition is presented in Fig. 3a,b,c. It is seen that the highest SFDR  $> 100$  dB is obtained with the bias current close to the critical current,  $i_b \rightarrow 1$ , see Fig. 3a. However, while the transfer coefficient for this bias current is also high (Fig. 3c), the bias flux is quite small (Fig. 3b), and thus the width of DSQUID working region is negligible.

Fortunately, there is a kind of plateau on  $i_b, \beta_l$  plane of parameters where  $i_b > 1$  and linearity is still rather high, SFDR  $> 90$  dB, see Fig. 3a. The example shown in Fig. 2a corresponds to the values of parameters:  $i_b = 1.02$ ,  $\beta_l = 0.35\pi$  at the boundary of this plateau providing both high enough bias flux,  $\phi_b = 0.3895\pi$ , and transfer coefficient,  $du/d\phi_s = 1.04$ , while linearity is SFDR = 92 dB and THD =  $6 \cdot 10^{-3}\%$ .

The chosen optimal bias flux corresponds to the width of the linear range equal to approximately a quarter of the width of SQUID working region,  $2\phi_a \approx \pi/8$ . The linearity increase is possible with decrease of the signal amplitude as shown in Fig. 4 by solid line. However, the bias flux should be additionally slightly tuned (see inset in Fig. 4). SFDR reaches 130 dB with peak-to-peak signal equal to 10% of the bias flux. SFDR obtained with constant bias flux is presented by dotted line.

While limitation of signal amplitude to a percent of DSQUID working region width makes utilization of the region I preferred, setting a fixed signal amplitude vice versa allows the usage of the region II. Optimization results obtained under utilization of the second condition ( $2\phi_a = \pi/8$ ) is presented in Fig. 3d,e,f. Fig. 3d shows that for inductance values

higher than  $\beta_l = 0.15\pi$  there are some values of the bias current  $i_b > 1$  providing high linearity of the voltage response, SFDR  $> 100$  dB (Fig. 3d), with the bias flux  $\phi_b$  close to  $\pi$  (Fig. 3e). Unfortunately, the transfer coefficient decreases with increase of SFDR, see Fig. 3d,f. For the previously chosen inductance,  $\beta_l = 0.35\pi$ , the optimal bias current is  $i_b = 1.108$  and with the bias flux equal to  $\phi_b = 0.8337\pi$  the transfer coefficient is  $du/d\phi_s = 0.22$ . Corresponding linearity is SFDR = 112 dB, THD =  $6 \cdot 10^{-4}\%$ . DSQUID voltage response for this set of parameters is presented in Fig. 2b.

Fig.5 shows SFDR dependence on deviation of DSQUID parameters from their optimal values,  $\delta i_b/i_b$ ,  $\delta \phi_b/\phi_b$ ,  $\delta \beta_l/\beta_l$ , for both examples shown in Fig. 2. It is seen that the linearity strongly depends on the bias current, see Fig.5a. One should set  $i_b$  with precision of  $\pm 0.1 - 0.2\%$  to keep SFDR not less than 10 dB from its maximum. At the same time for the same margin for SFDR the bias flux  $\phi_b$  can be set with an order less precision,  $\pm 1 - 2\%$ , see Fig.5b. Requirement for inductance value is even weaker (Fig.5c).

## 5. Discussion

The data shown in Fig. 5 indicate high requirements for the identity of SQUIDs parameters in DSQUID. The statistics of Josephson junctions critical currents fabricated by modern LTS fabrication process can be described approximately as Gaussian with standard deviation strongly depended on the junction size [34]. For the junctions with critical currents greater than  $180 \mu\text{A}$  (corresponding size is greater than  $1500 \text{ nm}$ ) the standard deviation is less than 1% for the process using 248-nm photolithography, see eq.(5) in [1]. Based on the data presented in Fig. 5a, we can estimate the real attainable linearity (SFDR) above 80 dB, accordingly.

Using conventional SQUID configuration one need restricting the width of the working range below  $0.1 \Phi_0$

to make THD less than 1% [35]. With a similar width of the working region,  $2\Phi_a = \Phi_0/8$ , DSQUID provides THD up to three orders better. By assuming the root mean square flux noise of  $\Phi_N = 10^{-6} \Phi_0/\text{Hz}^{-1/2}$ , one can obtain DSQUID dynamic range of about 100 dB/Hz $^{-1/2}$ . This means that with SFDR of an order of 100 dB DSQUID allows truly linear magnetic flux-to-voltage transformation since the distortions can be made lower than the noise floor.

SQA can be based on a DSQUID as far as the DSQUID is the DQC. The SQA formation can serve for the increase in dynamic range and transfer coefficient [12]. HTS-based SQUID arrays recently attracted attention due to the progress in fabrication of step-edge junctions [5] and the ones made with focused ion beam [8,36]. However, consideration of DSQUID-based array requires complication of the model with taking into account the noise and inductive coupling between cells [6,37]. Special attention should be paid to SQA matching with a load which was thoroughly studied in [38]. It was shown that DQC linearity is highly affected by the load and so high SFDR can be obtained with a proper serial-parallel connection of the cells keeping SQA impedance at least an order of magnitude lower than the impedance of the load.

## 6. Conclusion

We considered differential SQUID - a ‘‘DSQUID’’ possessing highly linear voltage response. The DSQUID is the differential connection of two identical SQUIDs. Two regions of SQUID voltage response suitable for linearization in DSQUID are identified. Arising tradeoff between the transfer coefficient and the width of the linearized region is revealed. Optimal values of the circuit parameters providing high linearity of the voltage response (SFDR > 100 dB and THD < 10 $^{-3}$ %) are found. The linearity dependence on deviation of the circuit parameters from their optimal values is studied. It is shown that the ultimate linearity comes at the cost of high identity of Josephson junctions (at the level of tenths of a percent) and high-precision current supply (up to the 3-d decimal place).

## 7. Acknowledgements

This work was supported by Grant No. 17-12-01079 of the Russian Science Foundation. Section 1 was written with the support of the RFBR grant 16-29-09515 ofi.m. V.I.R. acknowledges the Basis Foundation scholarship.

## Appendix

Expression (7) is approximation of DC SQUID voltage response shape. Analytical dependencies of its

parameters  $a$ ,  $\beta_l^*$  on  $i_b$ ,  $\beta_l$  are as follows [31,32]:

$$a = 2\kappa\nu(2i_b^2 - 1)/\xi, \quad \beta_l^* = \sqrt{\xi/\chi}, \quad (.1)$$

where

$$\kappa = \beta_l^{1.66}/(2.154\beta_l^{1.48} + 2.285), \quad (.2a)$$

$$\nu = \beta_l^{1.92}/(4.28\beta_l^{1.625} + 5.06), \quad (.2b)$$

$$\xi = -0.586\kappa + 2\nu + 4\kappa\nu(i_b^2 - 1), \quad (.2c)$$

$$\chi = 0.586i_b^2\kappa - \nu - 2\kappa\nu(i_b^2 - 1). \quad (.2d)$$

Parameters  $Q, Z$  of the Taylor series (8) are combinations of  $a$ ,  $\beta_l^*$  and  $i_b$ :

$$Q = a \left[ 1 + (\beta_l^* i_b)^{-2} \right]^{-1}, \quad (.3a)$$

$$Z = 1 - \left[ (\beta_l^* i_b)^2 - 3 \right] \left( 4i_b^2 \left[ 1 + (\beta_l^* i_b)^2 \right] \right)^{-1}. \quad (.3b)$$

## References

- [1] S. K. Tolpygo. Superconductor digital electronics: Scalability and energy efficiency issues. *Low Temperature Physics*, 42(5):361–379, 2016.
- [2] Niobium process. <http://www.hypres.com/foundry/niobium-process/>. Accessed: 2018-11-30.
- [3] I. I. Soloviev, N. V. Klenov, S. V. Bakurskiy, M. Y. Kupriyanov, A. L. Gudkov, and A. S. Sidorenko. Beyond Moore’s technologies: Operation principles of a superconductor alternative. *Beilstein Journal of Nanotechnology*, 8(1):2689–2710, 2017.
- [4] V. K. Semenov, Y. A. Polyakov, and S. K. Tolpygo. AC-biased shift registers as fabrication process benchmark circuits and flux trapping diagnostic tool. *IEEE Transactions on Applied Superconductivity*, 27(4):7856973, 2017.
- [5] S. Keenan, K. Hannam, E. Mitchell, J. Lazar, C. Lewis, A. Grancea, W. Purches, and C. Foley. Large high-temperature superconducting 2D SQIF arrays. In *European Conference on Applied Superconductivity (EUCAS), Geneva, Switzerland, 17-21 September 2017*, page EP172411, 2017.
- [6] V. K. Kornev, N. V. Kolotinskiy, A. V. Sharafiev, I. I. Soloviev, and O. A. Mukhanov. Broadband active electrically small superconductor antennas. *Superconductor Science and Technology*, 30(10):103001, 2017.
- [7] E. E. Mitchell, K. E. Hannam, J. Lazar, K. E. Leslie, C. J. Lewis, A. Grancea, S. T. Keenan, S. K. H. Lam, and C. P. Foley. 2D SQIF arrays using 20 000 YBCO high Rn Josephson junctions. *Superconductor Science and Technology*, 29(6):06LT01, 2016.
- [8] F. Coudo, E. R. Pawlowski, J. Kermorvant, J. Trastoy, D. Crt, Y. Lematre, B. Marcilhac, C. Ulysse, C. Feuillet-Palma, N. Bergeal, and J. Lesueur. High-Tc superconducting antenna for highly-sensitive microwave magnetometry. *arXiv*, page 1901.08786, 2019.
- [9] O. A. Mukhanov, D. Kirichenko, I. V. Vernik, T. V. Filippov, A. Kirichenko, R. Webber, V. Dotsenko, A. Talalaevskii, J. C. Tang, A. Sahu, P. Shevchenko, R. Miller, S. B. Kaplan, S. Sarwana, and D. Gupta. Superconductor digital-RF receiver systems. *IEICE Transactions on Electronics*, E91-C(3):306–317, 2008.
- [10] V. Zakosarenko, M. Schulz, A. Krueger, E. Heinz, S. Anders, K. Peiselt, T. May, E. Kreysa, G. Siringo, W. Esch, M. Starkloff, and H. G. Meyer. Time-domain multiplexed SQUID readout of a bolometer camera for APEX. *Superconductor Science and Technology*, 24(1):015011, 2011.

- [11] A. I. Braginski. Superconductor electronics: Status and outlook. *Journal of Superconductivity and Novel Magnetism*, 32(1):23–44, 2019.
- [12] V. K. Kornev, A. V. Sharafiev, I. I. Soloviev, N. V. Kolotinskiy, V. A. Scripka, and O. A. Mukhanov. Superconducting quantum arrays. *IEEE Transactions on Applied Superconductivity*, 24(4):06800001, 2014.
- [13] V. Kornev, A. Sharafiev, I. Soloviev, N. Kolotinskiy, and O. Mukhanov. Superconducting quantum arrays for broadband RF systems. In *Journal of Physics: Conference Series*, volume 507, page 042019, 2014.
- [14] V. K. Kornev, I. I. Soloviev, A. V. Sharafiev, N. V. Klenov, and O. A. Mukhanov. Active electrically small antenna based on superconducting quantum array. *IEEE Transactions on Applied Superconductivity*, 23(3):1800405, 2013.
- [15] V. K. Kornev, I. I. Soloviev, N. V. Klenov, and O. A. Mukhanov. Bi-SQUID: A novel linearization method for dc SQUID voltage response. *Superconductor Science and Technology*, 22(11):114011, 2009.
- [16] V. K. Kornev, I. I. Soloviev, N. V. Klenov, A. V. Sharafiev, and O. A. Mukhanov. Linear Bi-SQUID arrays for electrically small antennas. *IEEE Transactions on Applied Superconductivity*, 21(3 PART 1):713–716, 2011.
- [17] A. Sharafiev, I. Soloviev, V. Kornev, M. Schmelz, R. Stolz, V. Zakosarenko, S. Anders, and H. G. Meyer. Bi-SQUIDS with submicron cross-type Josephson tunnel junctions. *Superconductor Science and Technology*, 25(4):045001, 2012.
- [18] V. K. Kornev, A. V. Sharafiev, I. I. Soloviev, and O. A. Mukhanov. Signal and noise characteristics of bi-SQUID. *Superconductor Science and Technology*, 27(11):115009, 2014.
- [19] V. K. Kornev, I. I. Soloviev, N. V. Klenov, and N. V. Kolotinskiy. Design issues of HTS Bi-SQUID. *IEEE Transactions on Applied Superconductivity*, 26(5):7438807, 2016.
- [20] V. K. Kornev, N. V. Kolotinskiy, A. Y. Levochkina, and O. A. Mukhanov. Critical current spread and thermal noise in Bi-SQUID cells and arrays. *IEEE Transactions on Applied Superconductivity*, 27(4):7756342, 2017.
- [21] V. K. Kornev, N. V. Kolotinskiy, D. E. Bazulin, and O. A. Mukhanov. High-inductance Bi-SQUID. *IEEE Transactions on Applied Superconductivity*, 27(4):7752858, 2017.
- [22] V. K. Kornev, N. V. Kolotinskiy, D. E. Bazulin, and O. A. Mukhanov. High-linearity Bi-SQUID: Design map. *IEEE Transactions on Applied Superconductivity*, 28(7):1601905, 2018.
- [23] V. Kornev, N. Kolotinskiy, V. Skripka, A. Sharafiev, I. Soloviev, and O. Mukhanov. High linearity voltage response parallel-array cell. In *Journal of Physics: Conference Series*, volume 507, page 042018, 2014.
- [24] V. K. Kornev, I. I. Soloviev, N. V. Klenov, and O. A. Mukhanov. Design and experimental evaluation of SQIF arrays with linear voltage response. *IEEE Transactions on Applied Superconductivity*, 21(3 PART 1):394–398, 2011.
- [25] V. Kornev, I. Soloviev, N. Klenov, and O. Mukhanov. Progress in high-linearity multi-element Josephson structures. *Physica C: Superconductivity and its Applications*, 470(19):886–889, 2010.
- [26] V. K. Kornev, I. I. Soloviev, N. V. Klenov, and O. A. Mukhanov. High linearity SQIF-like Josephson junction structures. *IEEE Transactions on Applied Superconductivity*, 19(3):741–744, 2009.
- [27] V. K. Kornev, I. I. Soloviev, N. V. Klenov, T. V. Filippov, H. Engseth, and O. A. Mukhanov. Performance advantages and design issues of SQIFs for microwave applications. *IEEE Transactions on Applied Superconductivity*, 19(3):916–919, 2009.
- [28] G. V. Prokopenko, O. A. Mukhanov, A. Leese De Escobar, B. Taylor, M. C. De Andrade, S. Berggren, P. Longhini, A. Palacios, M. Nisenoff, and R. L. Fagaly. DC and RF measurements of serial Bi-SQUID arrays. *IEEE Transactions on Applied Superconductivity*, 23(3):6392883, 2013.
- [29] S. Berggren, G. Prokopenko, P. Longhini, A. Palacios, O. A. Mukhanov, A. L. de Escobar, B. J. Taylor, M. C. de Andrade, M. Nisenoff, R. L. Fagaly, T. Wong, E. Cho, E. Wong, and V. In. Development of 2-D Bi-SQUID arrays with high linearity. *IEEE Transactions on Applied Superconductivity*, 23(3):6407797, 2013.
- [30] D. Drung, J.-H. Storm, and J. Beyer. SQUID current sensor with differential output. *IEEE Transactions on Applied Superconductivity*, 23(3):1100204, 2013.
- [31] I. I. Soloviev, N. V. Klenov, A. E. Schegolev, S. V. Bakurskiy, M. Y. Kupriyanov, M. V. Tereshonok, and A. A. Golubov. Analytical description of low-Tc DC SQUID response and methods for its linearization. In *2017 16th International Superconductive Electronics Conference, ISEC 2017*, volume 2018-January, pages 1–3, 2018.
- [32] I. I. Soloviev, N. V. Klenov, A. E. Schegolev, S. V. Bakurskiy, and M. Y. Kupriyanov. Analytical derivation of DC SQUID response. *Superconductor Science and Technology*, 29(9):094005, 2016.
- [33] J. C. Lagarias, J. A. Reeds, M. H. Wright, and P. E. Wright. Convergence properties of the Nelder-Mead simplex method in low dimensions. *SIAM Journal on Optimization*, 9(1):112–147, 1998.
- [34] S. K. Tolpygo, V. Bolkhovskiy, T. J. Weir, L. M. Johnson, M. A. Gouker, and W. D. Oliver. Fabrication process and properties of fully-planarized deep-submicron Nb/Al-AlO<sub>x</sub>/Nb Josephson junctions for VLSI circuits. *IEEE Transactions on Applied Superconductivity*, 25(3):1101312, 2015.
- [35] M. Mueck and J. Clarke. Harmonic distortion and intermodulation products in the microstrip amplifier based on a superconducting quantum interference device. *Applied Physics Letters*, 78(23):3666–3668, 2001.
- [36] B. Mueller, M. Karrer, F. Limberger, M. Becker, B. Schroepfel, C. J. Burkhardt, R. Kleiner, E. Goldobin, and D. Koelle. Josephson junctions and SQUIDS created by focused helium ion beam irradiation of YBa<sub>2</sub>Cu<sub>3</sub>O<sub>7</sub>. *arXiv*, page 1901.08039v2, 2019.
- [37] P. Longhini, S. Berggren, A. L. de Escobar, A. Palacios, S. Rice, B. Taylor, V. In, O. A. Mukhanov, G. Prokopenko, M. Nisenoff, E. Wong, and M. C. De Andrade. Voltage response of non-uniform arrays of bi-superconductive quantum interference devices. *Journal of Applied Physics*, 111:093920, 2012.
- [38] V. K. Kornev, N. V. Kolotinskiy, V. A. Skripka, A. V. Sharafiev, and O. A. Mukhanov. Output power and loading of superconducting quantum array. *IEEE Transactions on Applied Superconductivity*, 25(3):1602005, 2015.